POLITECNICO DI TORINO
Repository ISTITUZIONALE

Novel biocompatible and resorbable UV-transparent phosphate glass based optical fiber

Original
Novel biocompatible and resorbable UV-transparent phosphate glass based optical fiber / CECI GINISTRELLI, E., Pugliese, D., Boetti, N.G., Novajra, G., Ambrosone, A., Lousteau, J., VITALE BROVARONE, C., Abrate, S., Milanese, D.. - In: OPTICAL MATERIALS EXPRESS. - ISSN 2159-3930. - ELETTRONICO. - 6:6(2016), pp. 2040-2051. [10.1364/OME.6.002040]

Availability:
This version is available at: 11583/2642917 since: 2016-10-15T15:34:45Z

Publisher:
Optical Society of America

Published
DOI:10.1364/OME.6.002040

Terms of use:

This article is made available under terms and conditions as specified in the corresponding bibliographic description in the repository

Publisher copyright

(Article begins on next page)

26 November 2026

Novel biocompatible and resorbable UV-transparent phosphate glass based optical fiber

Edoardo Ceci-Ginistrelli,[1] Diego Pugliese,[1] Nadia G. Boetti,[2,*] Giorgia Novajra,[1] Annarita Ambrosone,[1] Joris Lousteau,[3] Chiara Vitale-Brovarone,[1] Silvio Abrate,[2] and Daniel Milanese[1]

[1]*Politecnico di Torino, Institute of Materials Science and Engineering, Dipartimento di Scienza Applicata e Tecnologia (DISAT), Corso Duca degli Abruzzi 24, Torino, 10129, Italy*
[2]*Istituto Superiore Mario Boella, Via P. C. Boggio 61, Torino, 10134, Italy*
[3]*Optoelectronics Research Centre, University of Southampton, Southampton, SO17 1BJ, UK*
[*]*boetti@ismb.it*

Abstract: In this paper the first glass based resorbable optical fiber is manufactured and characterized, showing values of attenuation loss from one to two orders of magnitude lower than the polymeric based bioresorbable devices reported in literature. The fiber behaves as a single-mode waveguide at the lower limit of the first biological window (1300 nm) and as a multi-mode waveguide in the visible region (630 nm). Highly transparent calcium-phosphate glasses (PGs) are proposed as a new class of materials for biomedical optics, managing to combine for the first time in a vitreous material solubility in aqueous media, transparency in the near UV region, low intrinsic attenuation loss and thermal stability during fiber drawing. In-vitro tests in physiological conditions show dissolution kinetics of glass fibers in about a month.

© 2016 Optical Society of America

OCIS codes: (060.2290) Fiber materials; (060.2430) Fibers, single-mode; (160.2750) Glass and other amorphous materials; (160.1435) Biomaterials.

References and links

1. L. Brancaleon and H. Moseley, "Laser and non-laser light sources for photodynamic therapy," Lasers Med. Sci. **17**(3), 173–186 (2002).
2. A. K. Manocchi, P. Domachuk, F. G. Omenetto, and H. Yi, "Facile fabrication of gelatin-based biopolymeric optical waveguides," Biotechnol. Bioeng. **103**(4), 725–732 (2009).
3. H. Tao, J. M. Kainerstorfer, S. M. Siebert, E. M. Pritchard, A. Sassaroli, B. J. B. Panilaitis, M. A. Brenckle, J. J. Amsden, J. Levitt, S. Fantini, D. L. Kaplan, and F. G. Omenetto, "Implantable, multifunctional, bioresorbable optics," Proc. Natl. Acad. Sci. U.S.A. **109**(48), 19584–19589 (2012).
4. S. T. Parker, P. Domachuk, J. Amsden, J. Bressner, J. A. Lewis, D. L. Kaplan, and F. G. Omenetto, "Biocompatible silk printed optical waveguides," Adv. Mater. **21**(23), 2411–2415 (2009).
5. M. Choi, J. W. Choi, S. Kim, S. Nizamoglu, S. K. Hahn, and S. H. Yun, "Light-guiding hydrogels for cell-based sensing and optogenetic synthesis in vivo," Nat. Photonics **7**(12), 987–994 (2013).
6. A. Dupuis, N. Guo, Y. Gao, N. Godbout, S. Lacroix, C. Dubois, and M. Skorobogatiy, "Prospective for biodegradable microstructured optical fibers," Opt. Lett. **32**(2), 109–111 (2007).
7. E. A. Abou Neel, W. Chrzanowski, and J. C. Knowles, "Effect of increasing titanium dioxide content on bulk and surface properties of phosphate-based glasses," Acta Biomater. **4**(3), 523–534 (2008).
8. J. Burnie, T. Gilchrist, S. R. I. Duff, C. F. Drake, N. G. L. Harding, and A. J. Malcolm, "Controlled release glasses (C.R.G.) for biomedical uses," Biomaterials **2**(4), 244–246 (1981).
9. A. Hoppe, N. S. Güldal, and A. R. Boccaccini, "A review of the biological response to ionic dissolution products from bioactive glasses and glass-ceramics," Biomaterials **32**(11), 2757–2774 (2011).
10. N. Sharmin, A. J. Parsons, C. D. Rudd, and I. Ahmed, "Effect of boron oxide addition on fibre drawing, mechanical properties and dissolution behaviour of phosphate-based glass fibres with fixed 40, 45 and 50 mol% P_2O_5.," J. Biomater. Appl. **29**(5), 639–653 (2014).
11. C. Vitale-Brovarone, G. Novajra, D. Milanese, J. Lousteau, and J. C. Knowles, "Novel phosphate glasses with different amounts of TiO_2 for biomedical applications: Dissolution tests and proof of concept of fibre drawing," Mater. Sci. Eng. C **31**(2), 434–442 (2011).
12. E. A. Abou Neel, D. M. Pickup, S. P. Valappil, R. J. Newport, and J. C. Knowles, "Bioactive functional materials: a perspective on phosphate-based glasses," J. Mater. Chem. **19**(6), 690–701 (2009).

#262419 Received 1 Apr 2016; revised 17 May 2016; accepted 18 May 2016; published 23 May 2016

13. C. Vitale-Brovarone, G. Novajra, J. Lousteau, D. Milanese, S. Raimondo, and M. Fornaro, "Phosphate glass fibres and their role in neuronal polarization and axonal growth direction," Acta Biomater. **8**(3), 1125–1136 (2012).
14. G. Novajra, J. Lousteau, D. Milanese, and C. Vitale-Brovarone, "Resorbable hollow phosphate glass fibres as controlled release systems for biomedical applications," Mater. Lett. **99**, 125–127 (2013).
15. P. Hofmann, C. Voigtländer, S. Nolte, N. Peyghambarian, and A. Schülzgen, "550-mW output power from a narrow linewidth all-phosphate fiber laser," J. Lightwave Technol. **31**(5), 756–760 (2013).
16. N. G. Boetti, G. C. Scarpignato, J. Lousteau, D. Pugliese, L. Bastard, J.-E. Broquin, and D. Milanese, "High concentration Yb-Er co-doped phosphate glass for optical fiber amplification," J. Opt. **17**(6), 065705 (2015).
17. Y. Hu, S. Jiang, T. Luo, K. Seneschal, M. Morrell, F. Smektala, S. Honkanen, J. Lucas, and N. Peyghambarian, "Performance of high-concentration Er^{3+}-Yb^{3+}-codoped phosphate fiber amplifiers," IEEE Photonics Technol. Lett. **13**(7), 657–659 (2001).
18. C. Spiegelberg, J. Geng, Y. Hu, Y. Kaneda, S. Jiang, and N. Peyghambarian, "Low-noise narrow-linewidth fiber laser at 1550 nm (June 2003)," J. Lightwave Technol. **22**(1), 57–62 (2004).
19. Y.-W. Lee, M. J. F. Digonnet, S. Sinha, K. E. Urbanek, R. L. Byer, and S. Jiang, "High-power Yb^{3+}-doped phosphate fiber amplifier," J. Sel. Top. Quant. Electron. **15**(1), 93–102 (2009).
20. V. P. Gapontsev, S. M. Matitsin, A. A. Isineev, and V. B. Kravchenko, "Erbium glass lasers and their applications," Opt. Laser Technol. **14**(4), 189–196 (1982).
21. S. Jiang, M. J. Myers, and N. Peyghambarian, "Er^{3+} doped phosphate glasses and lasers," J. Non-Cryst. Solids **239**(1–3), 143–148 (1998).
22. D. Pugliese, N. G. Boetti, J. Lousteau, E. Ceci-Ginistrelli, E. Bertone, F. Geobaldo, and D. Milanese, "Concentration quenching in an Er-doped phosphate glass for compact optical lasers and amplifiers," J. Alloys Compd. **657**, 678–683 (2016).
23. S. Yliniemi, J. Albert, Q. Wang, and S. Honkanen, "UV-exposed Bragg gratings for laser applications in silver-sodium ion-exchanged phosphate glass waveguides," Opt. Express **14**(7), 2898–2903 (2006).
24. D. Grobnic, S. J. Mihailov, R. B. Walker, C. W. Smelser, C. Lafond, and A. Croteau, "Bragg gratings made with a femtosecond laser in heavily doped Er-Yb phosphate glass fiber," IEEE Photonics Technol. Lett. **19**(12), 943–945 (2007).
25. J. Massera, Y. Shpotyuk, F. Sabatier, T. Jouan, C. Boussard-Plédel, C. Roiland, B. Bureau, L. Petit, N. G. Boetti, D. Milanese, and L. Hupa, "Processing and characterization of novel borophosphate glasses and fibers for medical applications," J. Non-Cryst. Solids **425**, 52–60 (2015).
26. C.-K. Loong, K. Suzuya, D. L. Price, B. C. Sales, and L. A. Boatner, "Structure and dynamics of phosphate glasses: from ultra- to orthophosphate composition," Physica B **241–243**, 890–896 (1997).
27. R. K. Brow, "Review: the structure of simple phosphate glasses," J. Non-Cryst. Solids **263–264**(1), 1–28 (2000).
28. N. J. Lakhkar, I.-H. Lee, H.-W. Kim, V. Salih, I. B. Wall, and J. C. Knowles, "Bone formation controlled by biologically relevant inorganic ions: role and controlled delivery from phosphate-based glasses," Adv. Drug Deliv. Rev. **65**(4), 405–420 (2013).
29. F. A. Jerkins and H. E. White, *Foundamentals of Optics* (McGraw Hill, 1981).
30. A. M. Smith, M. C. Mancini, and S. Nie, "Bioimaging: second window for *in vivo* imaging," Nat. Nanotechnol. **4**(11), 710–711 (2009).
31. F. H. ElBatal and A. ElKheshen, "Preparation and characterization of some substituted bioglasses and their ceramic derivatives from the system SiO_2–Na_2O–CaO–P_2O_5 and effect of gamma irradiation," Mater. Chem. Phys. **110**(2–3), 352–362 (2008).
32. S. Pissadakis, A. Ikiades, P. Hua, A. Sheridan, and J. Wilkinson, "Photosensitivity of ion-exchanged Er-doped phosphate glass using 248nm excimer laser radiation," Opt. Express **12**(14), 3131–3136 (2004).
33. B. C. Bunker, G. W. Arnold, and J. A. Wilder, "Phosphate glass dissolution in aqueous solutions," J. Non-Cryst. Solids **64**(3), 291–316 (1984).
34. E. Mura, J. Lousteau, D. Milanese, S. Abrate, and V. M. Sglavo, "Phosphate glasses for optical fibers: Synthesis, characterization and mechanical properties," J. Non-Cryst. Solids **362**, 147–151 (2013).
35. Y. W. Lee, S. Sinha, M. J. F. Digonnet, R. L. Byer, and S. Jiang, "20 W single-mode Yb^{3+} -doped phosphate fiber laser," Opt. Lett. **31**(22), 3255–3257 (2006).
36. D. Yelin, D. Oron, S. Thiberge, E. Moses, and Y. Silberberg, "Multiphoton plasmon-resonance microscopy," Opt. Express **11**(12), 1385–1391 (2003).

1. Introduction

Recent developments in the field of biophotonics, for instance those in Photodynamic Therapy (PDT), optogenetics and biosensing, have raised interest in combining key biological functions to other technological properties, such as optical transparency, easy processing, bioresorbability, mechanical resistance and costs affordability. One research topic of growing interest concerns the manufacture of novel bioresorbable materials able to offer superior optical properties. The aim is to fabricate optical devices that can be fully resorbed once the therapeutic or diagnostic utility has been accomplished, eliminating the need of explant

#262419 Received 1 Apr 2016; revised 17 May 2016; accepted 18 May 2016; published 23 May 2016
© 2016 OSA

surgery. Such devices are of paramount interest in applications where light needs to be delivered in deep tissues of the human body without damaging the surrounding organs, as it happens in deep-tissue PDT applications or in-vivo sensing techniques [1].

In recent years, noticeable research efforts have led to the fabrication of some biodegradable waveguides for sensing purposes. Manocchi *et al.* [2] successfully developed a biopolymeric slab waveguide using an agarose - gelatin - agarose three layers structure, with a numerical aperture (NA) of 0.34 at the wavelength of 633 nm. Tao *et al*. [3] demonstrated the possibility of producing functional biomaterials for optical devices using natural silk proteins. Similarly, Parker *et al.* [4] produced a biocompatible silk printed optical waveguide, featuring an optical loss of 25 dB m^{-1} in the visible range. Choi *et al.* [5] successfully tested in-vivo a polyethylene glycol based hydrogel used both as a cell scaffold and as a waveguide. This device proved to be transparent up to 400 nm in the visible region and to have optical loss lower than 100 dB m^{-1}. A proof of concept biodegradable polymeric optical fiber was also published [6], featuring a 100 dB m^{-1} transmission loss at the wavelength of 630 nm. Although these are remarkable results, the proposed materials do not present as much versatility as bioresorbable glasses in terms of achievable optical properties, especially in terms of attenuation loss, refractive index and UV edge.

Over the years, phosphate glasses have proved to be a true contender as biomaterial for the development of bioresorbable commercial devices. They can be designed as to fully resorb in aqueous media, where the dissolution kinetics can be tailored through the glass composition itself [7]. The first bioresorbable phosphate glass, proposed in the early '80s for biomedical applications, was based on the calcium-phosphate glass system [8]. Since then, workers in the field have developed a better understanding of the biological compatibility of these materials [9]. Some glasses with P_2O_5 content around 50 mol% have proved to be resorbable, nontoxic and suitable for fiber drawing [10,11]. These materials have been studied for applications in hard and soft tissue regeneration, due to their interesting mechanical properties [10] and as their composition can be made compatible to that of human bone [12]. More recent studies from our research group have shown that phosphate glass fibers can be interesting devices in the treatment of peripheral nerve injuries since they allow directional growth of neural axons along fiber's axis [13,14].

Thanks to their excellent optical properties, phosphate glasses have been widely exploited for the development of laser sources and amplifiers [15–19]. These materials show high transparency in the UV-Visible/Near infrared (UV-Vis/NIR) region, refractive index values compatible with those of commercially available silica fibers and good thermal stability [20–22]. They are widely used for optical fiber drawing and suitable for Fiber Bragg Grating fabrication [23,24]. Despite these attractive features, only a few works have been reported so far on the development of glass compositions that combine bioresorbability, good optical properties and possibility to be drawn into fibers [25]. Nonetheless, we believe that a strong enhancement in the performance of bioresorbable optical devices is still obtainable by investigating the optical and dissolution behaviors of *ad hoc* designed PGs compositions for resorbable optical fibers.

The properties of PGs derive from their PO_4^{3-} tetrahedron structural unit, which consists of three bonding oxygens linked to neighboring tetrahedra and a terminal oxygen bonded to the phosphorous atom [26]. This structure is influenced by the presence of modifying oxides, that can depolymerize the structure of the glass converting the bridging oxygens into non-bridging oxygens. Depending on the type and concentration of modifying oxides, it is possible to obtain a wide range of structures, from cross linked Q^3 structures to isolated Q^0 structures. The variation in quality or in quantity of just one component of the glass will result in a different balance among these structures, thus in different properties of the material itself [27]. For this reason, modifying one feature of the material, for instance the dissolution kinetics, will typically cause changes to other properties of the material, such as the glass transition temperature or the refractive index. Typical biodegradable phosphate glasses also

#262419 Received 1 Apr 2016; revised 17 May 2016; accepted 18 May 2016; published 23 May 2016
© 2016 OSA

contain metallic ions which impair the glass transparency [9,11,28], and vice versa optical glasses are usually not suitable for in-vivo applications as they often contain some cytotoxic components. It is thus necessary to formulate new glass compositions in order to combine good optical properties and bioresorbability.

In this study the feasibility of combining the functionalities of PGs in the field of biomedical and optical materials was explored by fabricating and characterizing four different glasses. Suitable core and cladding compositions for optical fiber drawing are required to be stable against crystallization and to show similar glass transition temperatures (T_g) and low difference in terms of coefficients of thermal expansion (CTE). Glasses for applications in biophotonics and photomedicine also need a wide window of optical transparency, from the near ultraviolet (UV) to the near infrared (NIR) wavelength region, i.e. from 250 to about 2500 nm. This allows designing UV photosensitive materials suitable for Fiber Bragg Grating writing for biosensing application, through irradiation with UV or femtosecond laser sources.

All these properties need to be matched with suitable dissolution kinetics in physiological conditions (pH = 7.4, T = 37 °C). In this study a complete resorption of a 150 μm diameter fiber in about 30 days was targeted. Obviously, no release of any toxic ion or product should be observed during the dissolution process.

2. Materials and methods

2.1 Glass fabrication

Glass samples used in this work were synthesized by conventional melt-quenching method using chemicals (50% P_2O_5 – (30 - x)% CaO – (3 + x)% MgO – 11.5% Na_2O – 2.5% B_2O_3 – 3% SiO_2) with high purity level (99 + %). Four different glasses, named BPh1 ÷ BPh4, were obtained increasing the MgO molar concentration, ranging from 3 to 23 mol%, in substitution of CaO, ranging from 30 to 10 mol%. The chemicals were weighted and mixed within a dry box in order to minimize the hydroxyl ions (OH^-) content in the glass.

The batched chemicals, of the weight of 80 g each, were melted in alumina crucibles with a volume of about 150 ml at a temperature of 1200 °C for 1 h under controlled atmosphere; the melt was cast into a preheated brass mould, then annealed at a temperature around the transition temperature, T_g, for 12 h to relieve internal stresses, and finally cooled down slowly to room temperature. The obtained glasses were cut and optically polished to 1 mm-thick samples for optical and spectroscopic characterizations. Other samples with thicknesses of 12 and 5 mm were respectively used for density and CTE measurements.

2.2. Glass characterization

The density of the glasses was measured at room temperature by the Archimedes' method using distilled water as immersion fluid with an estimated error of 0.005 g cm^{-3}. Differential Thermal Analysis (DTA) was performed using a Netzsch DTA 404 PC Eos differential thermal analyzer up to 1200 °C with a heat rate of 5 °C min^{-1} in sealed Pt/Rh pans. An error of ± 3 °C was observed in measuring the characteristic temperatures.

The coefficient of thermal expansion was measured with a horizontal alumina dilatometer (Netzsch, DIL 402 PC) operating at 5 °C min^{-1} on 5 mm long specimens. The measure was automatically interrupted when shrinkage higher than 0.13% was achieved. The temperature reached when the shrinkage started was defined as the softening point (T_s) of the bulk glass. CTE values were calculated in the 200 ÷ 400 °C temperature range featuring an error of ± 0.1 $°C^{-1}$.

The refractive index of the glasses was measured at five different wavelengths (633, 855, 1061, 1312, 1533 nm) through a Metricon 2010 Prism Coupler. Two measurements per each wavelength were performed, with an estimated error of ± 0.001. The experimental values were fitted by the Cauchy's equation in order to calculate the variation of the refractive index

#262419 Received 1 Apr 2016; revised 17 May 2016; accepted 18 May 2016; published 23 May 2016
© 2016 OSA

in function of the wavelength. The obtained curve was used to interpolate the value of the refractive index at a wavelength of 980 nm.

UV-Vis/NIR absorption spectroscopy was performed at room temperature for wavelengths ranging from 180 to 3000 nm using a double beam scanning spectrophotometer (Varian Cary 500) in order to define the transparency and the UV edge of the glasses. The thickness of all the samples, polished with 3 μm diamond paste on both sides, was 1.00 ± 0.02 mm.

2.3. Fiber drawing

The furnace of the drawing tower consists of a stainless steel ring heated by induction operating at 248 kHz and delivering 170 W to reach the drawing temperature (SAET, Torino, Italy). Assuming the glass in a supercooled liquid state as an incompressible liquid, the diameter of the resulting fiber can be controlled by applying the mass flow conservation law. The parameters were set to manufacture 150 μm-thick cylindrical single material fibers, with an error of ± 6 μm on the diameter, employed for dissolution tests. The optical fiber preform was obtained by cane drawing of the core into a 4 mm diameter rod that fitted into a tube obtained by rotational casting at a rotation speed of 3000 rpm. A core/cladding rod of 4 mm diameter was then obtained by a second stretching and fit into a second tube identical to the first one. The so obtained final preform was finally drawn into an optical fiber, manufactured at the same conditions used for the fabrication of the single material fibers.

2.4. Dissolution tests

Dissolution tests were performed on glass fibers of the four different compositions. Fibers were soaked in Phosphate Buffered Saline solution (PBS, pH = 7.4) at a temperature of 37 °C with a solution volume/sample exposed area of 0.1 ml mm^{-2}. To calculate the exposed area of the fiber sample, fibers with a mean diameter D_f were considered as a single cylinder with the same diameter of the fiber and a length L, corresponding to the sum of single fibers lengths. The total surface area can be thus calculated as a function of the total weight of the fibers, density of the glass and mean diameter. A first experiment was set-up to evaluate the decrease in the fiber diameter. Three samples for each fiber composition were weighted and soaked in PBS. At different time points (3, 7, 14, 21 days) at least three fibers were removed from each container and dried. For each time point a measure of the fiber diameter on different fibers and in different positions of the fiber length (i.e. 15 measures for each fiber composition) was performed using an optical microscope (Nikon ECLIPSE E 50i) equipped with the image analysis software Q-Win. Refreshing of the medium was performed twice a week to simulate physiological fluid exchange.

In a second experiment the fibers weight loss and the pH change of the solution during fiber dissolution were studied. Three samples for each fiber composition were weighed and soaked in PBS in the same conditions used in the previous experiment and a measurement of the solution pH was performed twice a week (after 3, 7, 10, 14, 17, 21 days) before refreshing. After 21 days, the PBS solution was removed from the samples; the fibers were washed with bi-distilled water, dried and finally weighed. The weight loss was expressed as a percentage.

2.5. Optical fiber characterization

Fiber losses were measured by the cut-back technique using single-mode fiber pigtailed laser diode source at 633 nm (QFLD-660-10S) and 1300 nm (Infineon SBM 52414x). The laser was end face coupled to one of the active fiber cleaved ends. The attenuation value was calculated through linear least square fitting of the experimental data.

The modal properties of the optical fiber were investigated by taking a set of near-field images of the fiber cross-section at the wavelengths of 633 and 1300 nm, using butt-coupled fiber pigtailed laser diode sources.

#262419 Received 1 Apr 2016; revised 17 May 2016; accepted 18 May 2016; published 23 May 2016
© 2016 OSA

3. Results and discussion

3.1. Fabrication and characterization of the glasses

The host glass was *ad hoc* developed for this research with the aim to fabricate a robust but soluble glass, non-toxic and suitable for fiber drawing.

Differential Thermal Analysis (DTA) was carried out in order to measure the characteristic temperatures T_g (glass transition temperature) and T_x (onset crystallization temperature). T_g and T_x values allowed assessing a corresponding glass stability parameter around ΔT = 200 ± 6 °C, which suggests that these glasses are stable against devitrification and suitable for crystal free fiber drawing.

The CTE and the density values were also measured and the results are reported in Table 1.

It is possible to note that the variation in the MgO molar content has a little effect in changing the bulk density of the glasses. A decrease of the thermal stability and a limited increase of the glass transition temperature can also be observed with increasing the MgO content in the glass.

Table 1. Thermal and physical properties of the manufactured phosphate glasses: glass transition temperature T_g, crystallization temperature T_x, glass stability parameter ΔT, coefficient of thermal expansion CTE, softening temperature T_s and density ρ

Glass Label	MgO [mol%]	T_g [°C]	T_x [°C]	$\Delta T = T_x - T_g$ [°C]	CTE [10^{-6} °C^{-1}]	T_s [°C]	ρ [g cm^{-3}]
BPh1	3	435	658	223	12.6	467	2.606
BPh2	8	435	628	193	12.2	461	2.600
BPh3	15	442	632	190	12.0	471	2.598
BPh4	23	444	625	181	12.2	477	2.589

Figure 1 reports the variation of the refractive index of the glasses at 633, 980, and 1312 nm, respectively, as a function of the MgO content. The refractive indexes were measured directly on the material by the prism coupling method, except for the value at 980 nm, which was calculated using the Cauchy's equation [29] on the basis of the experimental data. The range of wavelengths of interest was limited to values laying between 633 and 1312 nm, corresponding to the NIR biological optical window (from 600 up to 1300 nm) [30]. The refractive index values appear to decrease linearly with increasing MgO molar content in substitution to CaO in the composition of the glass.

With the aim to fabricate a step-index optical fiber where the core is made from glass BPh1, the corresponding numerical aperture (NA) values at 633 nm are reported in Table 2 considering BPh2, BPh3 and BPh4 as possible cladding glass candidates.

It can be noticed in Fig. 1 that it is possible to design a low NA optical fiber choosing adequately the amount of MgO content in the glass by interpolating the refractive index data. This also allows perspective fabrication of single-mode optical fibers in the NIR.

In order to manufacture an optical fiber, obtaining materials that are thermo-mechanically compatible is of crucial importance. In this specific case, it is worth noting that the measured physical properties do not change significantly by varying the MgO content in the glass: a significant variation of the refractive index of each glass pair can be observed without affecting the T_g and CTE values, thus minimizing the residual stress in the fiber.

#262419 Received 1 Apr 2016; revised 17 May 2016; accepted 18 May 2016; published 23 May 2016
© 2016 OSA

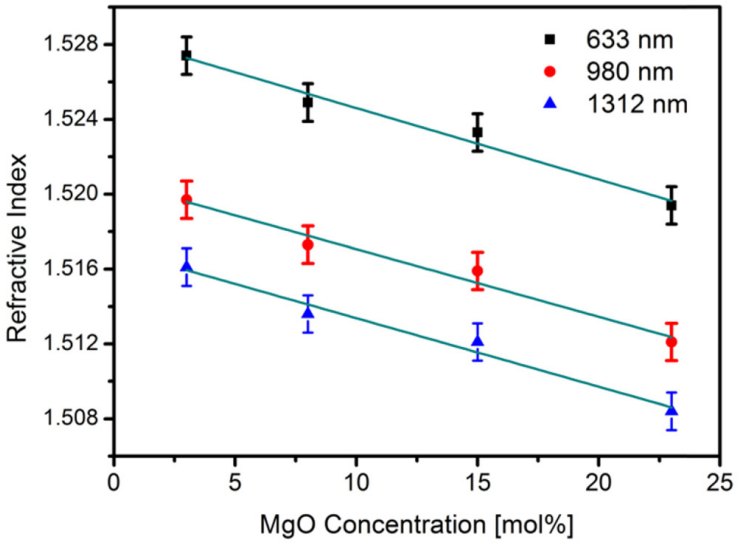

Fig. 1. Refractive index values of the prepared glasses as a function of the MgO content at three different wavelengths (633, 980, 1312 nm). The symbols represent the experimental data, while continuous green lines are the linear fitting curves.

Table 2. Numerical apertures at 633 nm of glass BPh1 coupled to BPh2, BPh3 and BPh4

Glass label	Refractive Index (at 633 nm)	NA (at 633 nm)
BPh1/BPh2	1.527/1.525	0.087
BPh1/BPh3	1.527/1.523	0.112
BPh1/BPh4	1.527/1.520	0.156

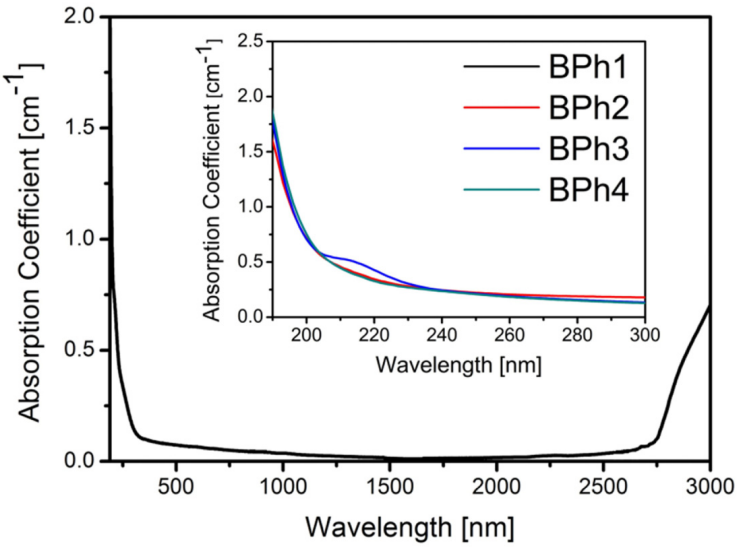

Fig. 2. Absorption coefficient spectrum of BPh1 glass; the inset shows the zoom-up of the spectra of all the glass compositions in the region between 190 and 300 nm.

#262419 Received 1 Apr 2016; revised 17 May 2016; accepted 18 May 2016; published 23 May 2016
© 2016 OSA

The transparency of the glass materials BPh1, BPh2, BPh3 and BPh4 was assessed through UV-Vis/NIR measurements. It is worthwhile noting that the values measured for the absorption coefficient should not be considered as an intrinsic property of the material, as a strong influence of the surface quality of the sample is present. A typical spectrum is presented in Fig. 2 for BPh1 glass. In the inset of the same figure the absorption spectra of all the glasses in the wavelength region between 190 and 300 nm are reported, in order to show the UV edge of the different compositions. It can be observed that all glasses show a similar transparency from the NIR down to the near UV (from 2500 down to 240 nm), thus broader than that reported for polymeric waveguides [5,6] and most common bioglasses [31], which are usually opaque under 400 nm. This opens the prospect of using different light wavelengths, from UV to NIR regions, for various biomedical applications. The relative transparency of the glass in the near UV is also a requested feature to induce significant changes in the refractive index under intense irradiation [32]. This effect is exploited to manufacture Fiber Bragg Gratings, which are of great interest in the field of biosensing.

3.2 Fabrication and characterization of single material glass fibers

Single material fibers of 150 ± 6 µm diameter were fabricated for dissolution tests in physiological conditions (37 °C, pH = 7.4). For each glass composition BPh1, BPh2, BPh3 and BPh4, the fibers were drawn from cylindrical glass rods of 11 mm in diameter and 120 mm in length and soaked in PBS solution for 21 days. In a first dissolution experiment, the decrease in diameter of the fibers was periodically monitored over the whole dissolution time. In a second dissolution experiment, the pH change of the solution during fiber dissolution was periodically monitored during the 21 days of the test, and the total weight loss was measured for each composition at the end of the experiment.

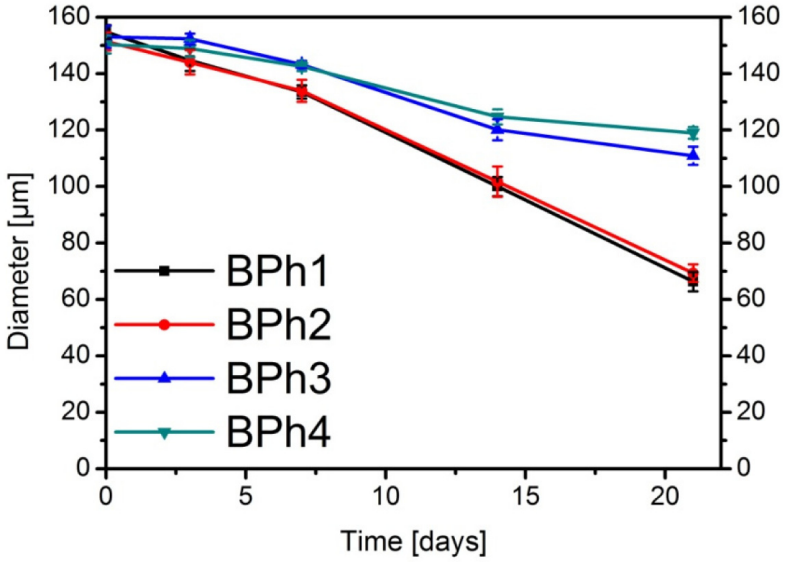

Fig. 3. Diameter values of the prepared glass fibers after 3, 7, 14 and 21 days of soaking in PBS.

#262419 Received 1 Apr 2016; revised 17 May 2016; accepted 18 May 2016; published 23 May 2016
© 2016 OSA

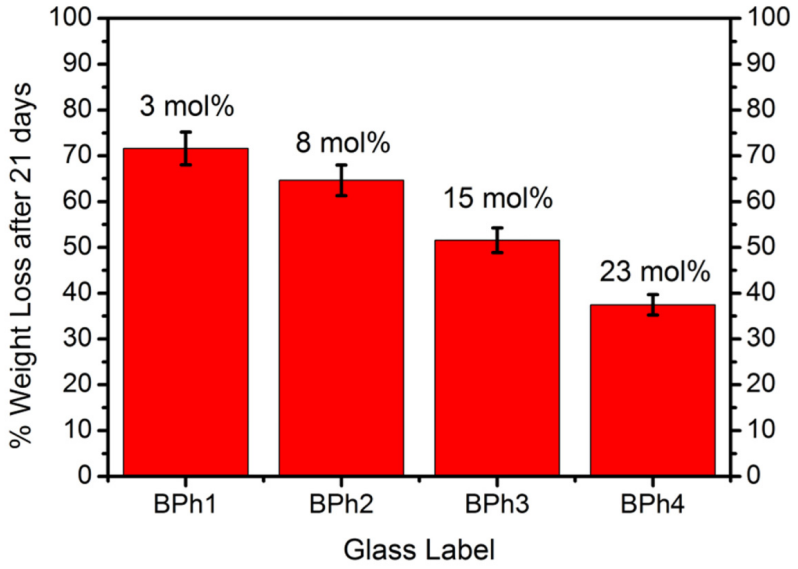

Fig. 4. Weight loss percentage of the fibers of the different compositions after 21 days of soaking in PBS. For the benefit of the reader, the MgO molar concentration values are reported on top of the histogram bars.

Overall, the results show that the initial target of a complete dissolution within 30 days in PBS can be considered achieved for the BPh1 and BPh2 compositions, while BPh3 and BPh4 show slower dissolution rates. However, it is of high interest noting how the dissolution kinetics can be tailored by modifying the glass composition. The results of the dissolution experiments 1 and 2 are reported in Fig. 3 and Fig. 4, respectively. It clearly appears that a decrease in glass solubility occurs when replacing MgO with CaO. This observation indicates a higher strengthening effect of MgO with respect to CaO in the glass network. Ca^{2+} and Mg^{2+} are both divalent cations able to create ionic-crosslinks between the non-bridging oxygens of two different chains, contributing to an increase in the durability of the glass if compared to monovalent cations, such as Na^{+} [33]. However, stronger bonds can be created by Mg^{2+} as a result of the smaller ionic radius, and thus higher field strength, of Mg^{2+} (72 Å) compared to that of Ca^{2+} (99 Å). The change in dissolution rate is not linear with the MgO molar concentration. In fact, similar behavior was observed for BPh1 and BPh2. These materials are characterized by a MgO content of 3 and 8 mol%, respectively, and show a decrease in diameter of 89 and 82 μm, corresponding to a dissolution of the fiber surface of about 2 μm day^{-1}. On the other side BPh3 and BPh4 present MgO molar concentration equal to 15 and 23 mol% and show a decrease in diameter of 42 and 31 μm, respectively. This corresponds to a surface dissolution rate of 0.7 and 1.0 μm day^{-1}, respectively. To a careful analysis of the results, a slight discrepancy between the weight losses reported in Fig. 4 and the diameter reduction after 21 days (see Fig. 3) can be observed. This is due to a systematic error in the measurement, related most probably to the imperfect drying of the residual fibers or to a scarce sensitivity of the balance for such small quantities. In any case the weight loss experiment, although less accurate, confirms the trend observed in Fig. 3.

The in-vitro dissolution test demonstrated that the developed PGs are soluble in aqueous media in simulated physiological conditions. Although the kinetics of dissolution in-vitro is not comparable to that in-vivo, due to the intrinsic difference of a living organism compared to any simulated solution, yet it is possible to compare the dissolution rates obtained for the respective glass compositions developed in this work. A small decrease in the dissolution speed of the glass can be noted when the MgO concentration in the glass increases, in response to the stabilization of the glass network. This observation agrees with the thermal

#262419 Received 1 Apr 2016; revised 17 May 2016; accepted 18 May 2016; published 23 May 2016
© 2016 OSA

properties of the glasses, which show a slight increase in T_g with increasing MgO molar content. Both for the glass dissolution rate and the glass transition temperature T_g, no linear correlation could be observed with respect to MgO molar concentration.

As one can observe in Fig. 5, a slight change in pH was caused by the dissolution of the fibers for all glasses, however remaining in the physiological range (from 7.2 up to 7.6). This is a necessary factor in order to ensure that the dissolution of devices made from these glasses is well tolerated by the organism and is an important feature for the exploitation of this material for biomedical applications.

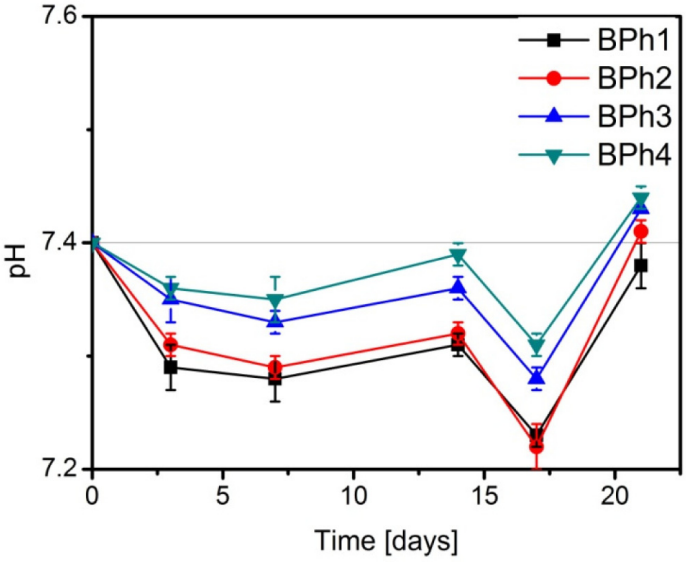

Fig. 5. pH variations in PBS during the dissolution test.

3.3 Fabrication and characterization of the bioresorbable optical fiber

Following the development of bioresorbable glasses with suitable optical properties, the second goal of this investigation was to develop an optical fiber from the latter materials. The core/cladding pair was selected on the basis of previous optical characterization: BPh1 and BPh2 were chosen as core and cladding components, respectively, due to the adequate value of NA, suitable for single-mode fiber drawing. The bioresorbable optical fiber was manufactured by preform drawing, where the core/cladding glass structured preform was developed through the rod-in-tube technique. For this, a 4 mm diameter rod of core glass BPh1 was obtained by drawing an 11 mm diameter preform. Two cladding tubes with an outer diameter of 12 mm and an internal diameter of 4.5 mm were fabricated by rotational casting using in-house developed equipment [34].

Optical microscopy was performed on different sections of the fiber to assess its dimension and its overall quality. A particular attention was given to the examination of the core/cladding interface quality. A typical micrograph of the fiber cross-section is shown in Fig. 6. The diameter of the fiber is 120 µm and the core diameter is 12 µm, as expected from the preform design and engineering. A homogeneous material and a good interface adhesion between core and cladding can be observed, thus demonstrating the thermo-mechanical compatibility of the two glasses BPh1 and BPh2.

#262419 Received 1 Apr 2016; revised 17 May 2016; accepted 18 May 2016; published 23 May 2016
© 2016 OSA

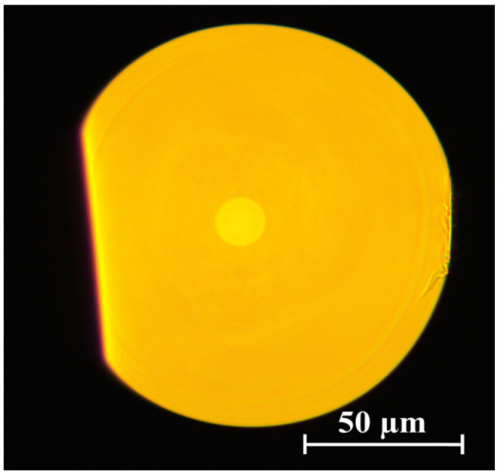

Fig. 6. Section of the optical fiber.

The surface quality of the core/cladding interface of the step-index fiber is an important parameter to be considered when fabricating an optical device, as it heavily influences the optical loss. The rotational casting procedure proves to be an effective and reproducible technique to obtain good quality internal surface of the cladding tubes. This, together with a careful polishing of the core glass rod surface, allows for obtaining excellent core/cladding interface.

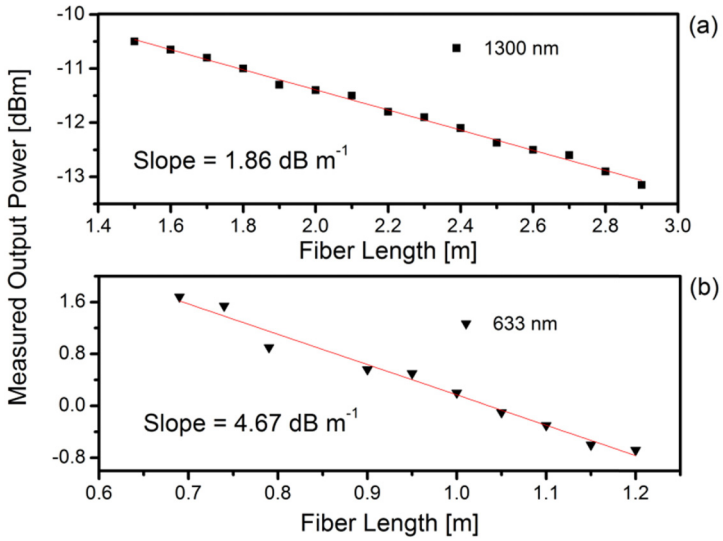

Fig. 7. Attenuation loss of the optical fiber at 1300 nm (a) and at 633 nm (b).

The attenuation loss of the fiber was measured by cut-back method on fiber samples of different lengths using laser diode sources operating at the edges of the first biological window (from 600 to 1300 nm). The results, reported in Fig. 7, show attenuation loss coefficients of 1.9 and 4.7 dB m^{-1}, measured respectively at 1300 and 633 nm. These values are one to two orders of magnitude lower in the decibel scale than those published so far for bioresorbable waveguides and can be imputed mainly to the defects at the core/cladding interface of the fiber [4–6]. These values are in line with the typical loss values associated to PGs optical fibers [35], thus showing the advantage in using PGs based optical waveguides

#262419 Received 1 Apr 2016; revised 17 May 2016; accepted 18 May 2016; published 23 May 2016
© 2016 OSA

for bioresorbable optics and validating the excellent quality of the bulk material. Near-field imaging of the fiber output was recorded using an IR camera to assess the modal properties of the fiber. The fiber operates in the single-mode regime at a wavelength of 1300 nm, while multi-mode behavior can be observed at 633 nm (see Fig. 8). The estimated values of the V number, based on the refractive index measurements and the fiber size, confirm the observed behavior (V = 2.29 at 1500 nm, V = 2.44 at 1300 nm, V = 8.23 at 633 nm).

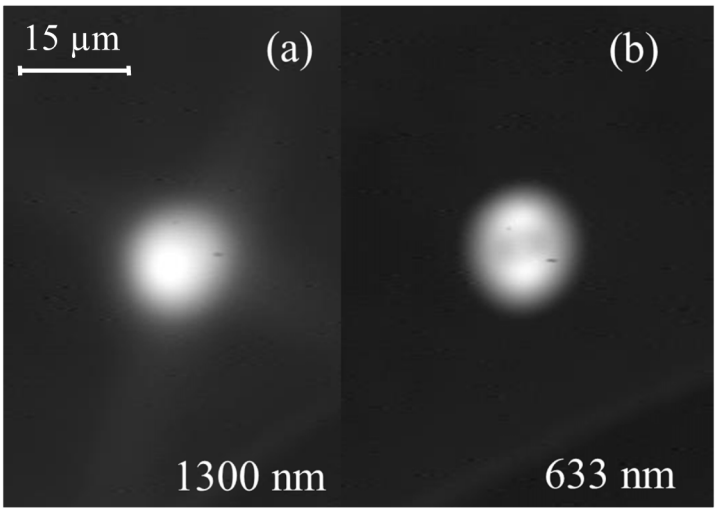

Fig. 8. Near-field pictures show only the fundamental mode propagating at 1300 nm (a), while higher order modes can be observed at 633 nm (b).

4. Conclusion

In conclusion, we demonstrate that calcium-phosphate glasses offer an exclusive combination of optical and biological properties, making these materials attractive for the fabrication of bioresorbable devices for various biomedical applications. In detail, the compositions developed *ad hoc* for this research present a wide window of transparency from UV to near IR region and refractive index adjustable to different values without a significant change in the thermal properties. The materials developed are suited for fiber drawing and are soluble in simulated biological environment (PBS, pH = 7.4 at 37 °C). We proposed a simple and large-scale extendable method for the manufacture of a resorbable optical fiber, which was fabricated and tested as a proof of feasibility. The device showed to be effective in guiding light at different wavelengths in the first biological optical window and its power losses resulted to be the lowest measured in literature on bioresorbable optical waveguides. Further studies are ongoing in order to assess the mechanical properties of the fibers and the photosensitivity of the PGs, in view of manufacturing FBGs based biosensors. Moreover, these preliminary results open some interesting prospective to exploit glass based bioresorbable optical fibers as waveguides and sources for PDT treatments. Taking advantage of their unique combination of properties, we believe that calcium-phosphate glasses will be of major interest in the fabrication of new devices for biophotonics and photomedicine, contributing significantly to the technological progress in these fields.

Acknowledgments

The authors acknowledge the COST Action MP1401 “Advanced Fiber Laser and Coherent Source as tools for Society, Manufacturing and Lifescience” for the partial support of this research effort. J. Lousteau acknowledges funding from the EC People Programme (Marie Curie Sklodowska Actions) under Grant Agreement n. 659092 (WISDOM).